ELSEVIER

Polymer 41 (2000) 5855–5864

polymer

# Simultaneous biaxial drawing of poly (ϵ-caprolactone) films

C.S. Ng[a], S.H. Teoh[a,*], T.S. Chung[b,c], D.W. Hutmacher[a]

[a]*Laboratory for Biomedical Engineering, Institute of Engineering Science & BIOMAT Center, Department of Mechanical & Production Engineering, National University of Singapore, 10 Kent Ridge Crescent, Singapore, 119260*

[b]*Department of Chemical & Environmental Engineering, National University of Singapore, 10 Kent Ridge Crescent, Singapore 119260*

[c]*Institute of Materials Research & Engineering, National University of Singapore, 10 Kent Ridge Crescent, Singapore 119260*

Received 5 August 1999; received in revised form 27 September 1999; accepted 5 October 1999

**Abstract**

The objective in our study was to investigate the biaxial drawing of Poly (ϵ-caprolactone) (PCL), a bioerodable polyester that is flexible and elastomeric. PCL films were fabricated using solution casting and melt-pressing methods, and biaxially drawn to draw ratio of $3 \times 3$. The morphology, mechanical properties and gas permeability changes of the undrawn and drawn films were studied. Results showed that even at the low draw ratio used, a fibrillar morphology developed in the films, interspersed with undrawn material. The tensile strengths of the drawn films were also improved by 50–160%. The solution-cast films have higher gas permeabilities (20-fold), with Knudsen flow character, than melt pressed films. This higher gas permeability was attributed to the presence of microvoids and drawing defects. Permeability was reduced in the melt-pressed films and oxygen was found to permeate three times faster than nitrogen. Biaxial drawing increased the gas permeability slightly but selectivity remained unchanged. 

*Keywords*: Simultaneous biaxial drawing; Biodegradable polymer; Characterisation

## 1. Introduction

Biaxial drawing is an important industrial process for producing thin films with improved physical properties [1]. The tensile strength and modulus are improved due to the induced orientation of polymer fibrils by the drawing process. Biaixally drawn films have been widely used in packaging applications. Unlike uniaxial drawing, where the improvement is limited to along the drawing direction, biaxial drawing produces films that are stronger in both the longitudinal and lateral directions. Hence due to the superior mechanical properties, biaxially drawn films are produced in the polymer industry. Among the commercially important polymeric materials, the biaxial drawing of films of polyethylene, polypropylene and poly (ethylene terepthalate) are the best studied. Sakai et al. investigated structural changes [2], development of fibrillar morphology [3] and mechanical properties [4] in the biaxial drawing of ultra-high molecular weight polyethylene (UHMWPE) films. In the studies on biaxially drawn polypropylene, Taraiya et al. [5] investigated the barrier properties whereas Chu et al. [6] studied the formation of microvoids. Gerrits et al. [7] and Zhu et al. [8] evaluated the microporosity generated from biaxially drawing UHMWPE and polypropylene, respectively. For the fabrication of the specimens, different processing techniques have been applied. Sakai et al. and Gerrits et al. used films obtained from solution casting whereas those who worked on polypropylene prepared their films using melt pressing. However, until now, few have addressed biodegradable polymers in specific.

The research on biodegradable and bioerodable polymers has been rapidly progressing over the past few years. Apart from tackling environmental litter issues, there is also intense interest in biomedical applications, especially tissue engineering and controlled drug delivery. In a recent review paper [9], Amass et al. have indicated that speciality packaging for biomedical products can also constitute a market for biodegradable polymers. Biodegradable polymers that are also biocompatible, such as poly lactides, poly glycolides and poly (ϵ-caprolactone), are ideal materials for pharmaceutical products and wound dressings.

Poly(ϵ-caprolactone) (PCL) is a semicrystalline, biodegradable polymer belonging to the aliphatic polyesters family. The ester group is responsible for the chemical degradability of the polymer through hydrolysis [10]. Studies [11,12] have also shown that PCL is biocompatible and its degradation by-products, developed by bulk erosion,

* Corresponding author. Tel.: +65-874-6345; fax: +65-777-3537.
*E-mail address:* mpetsh@nus.edu.sg (S.H. Teoh)

0032-3861/00/$ - see front matter 
PII: S0032-3861(99)00760-0

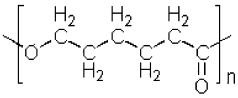

Fig. 1. Chemical structure of PCL.

are non-toxic. This makes it a potential material candidate in biomedical applications, like development of membranes, foils and sutures [13].

The chemical structure of PCL is shown in Fig. 1. The linear chains of methylene groups impart a hydrophobic nature to the polymer. In general, the polymer bears similarity in characteristics to polyethylene. PCL has a low melting point ($T_m$) of 60°C and a glass transition temperature ($T_g$) of −60°C. Due to its low $T_g$, PCL is always in a rubbery state at room temperature. Compared to the better known aliphatic biodegradable polyesters, such as poly lactides and poly glycolides, this is an unusual property that imparts high drawability and processing ease to PCL.

In this work, PCL thin films, prepared under two different processing conditions: solution casting and melt pressing were biaxially drawn. We report on the mechanical, morphology and gas permeability characterisations of the drawns films. The results were compared and discussed in relation with the undrawn films.

## 2. Materials and methods

### *2.1. Film preparation*

PCL thin films were prepared using a standard solution-casting method. PCL ($M_n$ 80 000) was purchased from Sigma–Aldrich Company and used as received. PCL pellets were dissolved in methylene chloride (6% (w/w)) and casted over glass sheets. The solvent was removed by slow evaporation (>6 h). The films were further dried in vacuum at room temperature for two days. Films of diameter 210 mm with a thickness of 100–110 μm were obtained.

### *2.2. Heat pressing and biaxial drawing*

To achieve the processing conditions below and above the melting temperature of PCL, the as-cast films were heat-pressed at 55°C (pressure—4 MPa) and 80°C (pressure—0.4 MPa) for 10 min. A Cavar Heat Press with a platen area of 36 in.$^2$ (0.023 m$^2$) was used. The films pressed at 80°C were equivalent to a melt-pressed film since PCL melts at 60°C. Pressing at 55°C did not melt the PCL films. Hence the morphology from the solution casting process was preserved. However, the heat press process was necessary to improve film uniformity, and to reduce defects, which would negatively influence the biaxial drawing process. All pressed films were quenched into ice water immediately after removal from the hot press. The pressed films were cut to 7 × 7 cm for biaxial drawing. For identification

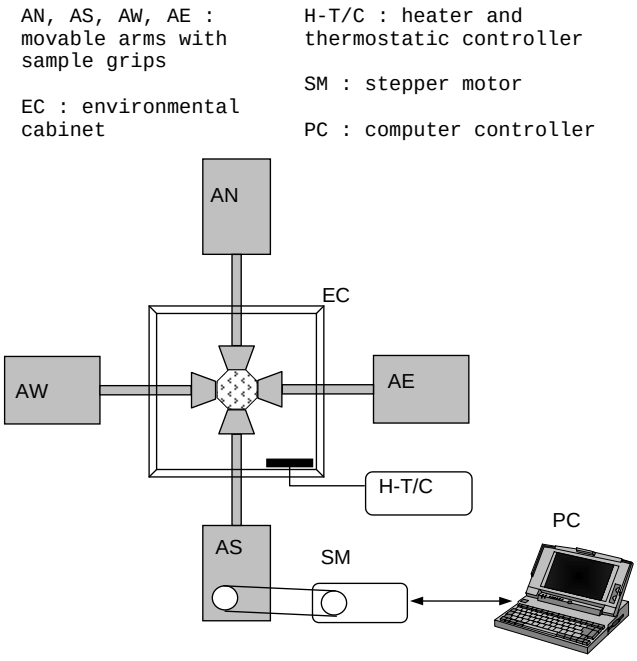


Fig. 2. Schematic set-up of biaxial drawing apparatus.

purposes, samples reported in this paper will be called "PCL-T" to denote films after heat pressed at a temperature of $T$°C.

The films were biaxially drawn using a biaxial drawing apparatus designed and built in-house (Fig. 2). It consists of sample grips mounted at the ends of four movable arms. The film sample (square geometry) was held at the four corners by the sample grips. The arms were arranged in pairs in a north–south and east–west axes fashion. An axle connects each pair of arms, and a system of gears and screws provided displacement of the arms. To ensure synchronised and equal displacement of the four arms, the two axles were coupled via a bevel gear. A stepper motor linked the south-end gear via a driving belt. A computer controlled the stepper motor and provided different strain rates for drawing. To allow drawing at elevated temperatures, the set-up was enclosed in an insulated cabinet with a thermostat-controlled heater. Samples were pre-heated for 30 min before drawing. The temperature during pre-heat and drawing was 53 ± 1°C.

All samples were processed using a drawing speed of 200 mm/min. Non-uniform drawing was observed at draw ratios less than 2 × 2, especially for PCL-80 samples. The films tended to rupture at draw ratios close to 4 × 4. Therefore, the draw ratios for all samples were fixed at 3 × 3. Draw ratio was determined from the displacement of pre-placed ink marks on the drawn samples. Biaxial deformation was observed in the centre portion of the film while the edges underwent uniaxial drawing. Hence, subsequent characterisations were made only on material obtained from the centre of the biaxially drawn film. Thin transparent

film specimens were obtained after drawing. The thicknesses of the films were 5–15 μm. Biaxially drawn samples will be called "PCL-T-BXD" in this paper, where $T$ is the heat press temperature.

### 2.3. Characterisation

The following characterisations were performed on four groups of PCL films, namely: PCL-55, PCL-55-BXD, PCL-80 and PCL-80-BXD.

#### 2.3.1. Morphology

The morphology was examined using an Olympus BX50 transmission optical microscope. Images were captured with a video camera and digitally stored on a hard disk.

Atomic force microscopy (AFM) was performed using a Topometrix TMX2000 system equipped with a dry scanner probe tip. The contact mode was used during scanning. All scans were performed over an area of $10 \times 10$ and $5 \times 5$ μm. Representative scans from three different films of each group were collected.

#### 2.3.2. Tensile testing

The tensile properties at room temperature were determined using an Instron Universal tensile tester (Model 4302 & 5542). The sample size of each group was 10. As PCL-55 and PCL-80 samples were thicker than the drawn films, they were tested on model 4302 with a 1 KN capacity load cell. This model has pneumatic grips, which could provide a stronger grip on the thicker samples, thus minimising slippage. The model also has a longer cross-head travel, which is necessary to accommodate the high break extensions (>600%) of the samples. The biaxially drawn films, being thinner, were tested on model 5542 (for miniature samples) using a 5 N capacity load cell. The grip separation was set at 30 mm and a testing speed of 5 mm/min was used. The biaxially drawn films were tensile tested at 45°C to the biaxial draw directions.

The thicknesses of the films were measured using a spacer with a known thickness (1 mm) as described by Teoh et al. [14]. The spacer provided large contact area over the soft films and prevented extraneous compression, commonly seen in conventional one-point contact measurements. Two instruments were used for the thickness measurements. For the thicker PCL-55 and PCL-80 films, a Carycompar B Vertical comparator (type Y 150) that has an accuracy of 1 μm was used. The thicknesses of the thinner films after biaxial drawing were measured with a Sigma Mechanical comparator (MC 201-15) to the nearest 0.5 μm.

The engineering stress ($\sigma$) was defined as the ratio of load ($L$) to the sample cross-sectional area ($A$) ($\sigma = L/A$). The percentage strain ($\lambda$) was computed from $[(l - l_0)/l_0] \times 100\%$, where $l$ was the total extension measured from the grip displacement and $l_0$ the initial gauge length (30 mm). The initial Young's modulus was calculated from the initial slope of the stress–strain curve. The tensile strength was obtained from the stress recorded at film fracture.

#### 2.3.3. Differential scanning calorimetry

The changes in the thermal response were studied using a Perkin–Elmer Pyris-1 DSC. The instrument was calibrated with Indium and Zinc standards. The sample weight used was 5–6 mg. All samples were scanned from 23 to 80°C at a ramp rate of 5°C/min, using nitrogen as purge gas. A total of three samples were analysed in each group.

#### 2.3.4. Gas permeability measurement

The gas permeability was measured using a constant volume, variable pressure method. Details of the experimental set-up may be found elsewhere [15]. The measurement was performed at 25°C with gases of $O_2$ and $N_2$. An upstream pressure of 72 and 135 cmHg was used for PCL-55 and PCL-80 groups, respectively, including biaxially drawn samples. Due to the extremely thin film thickness of PCL-55-BXD samples, a lower pressure had to be used so that the pressure transducer would not be damaged in case film rupture occurs during testing. The gas permeability coefficient $P$ (Barrer: $cm^3$(STP) cm/s $cm^2$ cmHg) was calculated from the slope ($dP/dt$) at a steady state using Eq. (1).

$$P = \frac{273 \times 10^{10}}{760} \frac{Vl}{AT\left(\frac{p_2 \times 76}{14.7}\right)} \frac{dP_1}{dt} \tag{1}$$

where $V$ is the volume of downstream compartment ($cm^3$), $T$ is the temperature (K), $A$ is the effective film permeation area ($cm^2$), $l$ is the film thickness (cm), $P_2$ is the upstream pressure (psia), and $dP_1/dt$ is the rate of downstream pressure build-up (cmHg/s).

Permselectivity ($\alpha$) between two gases was calculated as follows:

$$\alpha_{X/Y} = \frac{P_X}{P_Y} \tag{2}$$

where, $P_X$ is the permeability coefficient of gas X and $P_Y$ is the permeability coefficient of gas Y.

## 3. Results and discussion

### 3.1. Bulk morphology from optical microscopy

The optical micrographs of the PCL samples at different heat pressing temperatures (before and after biaxial drawing) are shown in Fig. 3. PCL-55 samples exhibited a spherulitic structure with large spherulites. This spherulitic structure is a result of crystal growth from the slow solvent evaporation during solution casting process [16]. In contrast, spherulites were not observed after pressing PCL

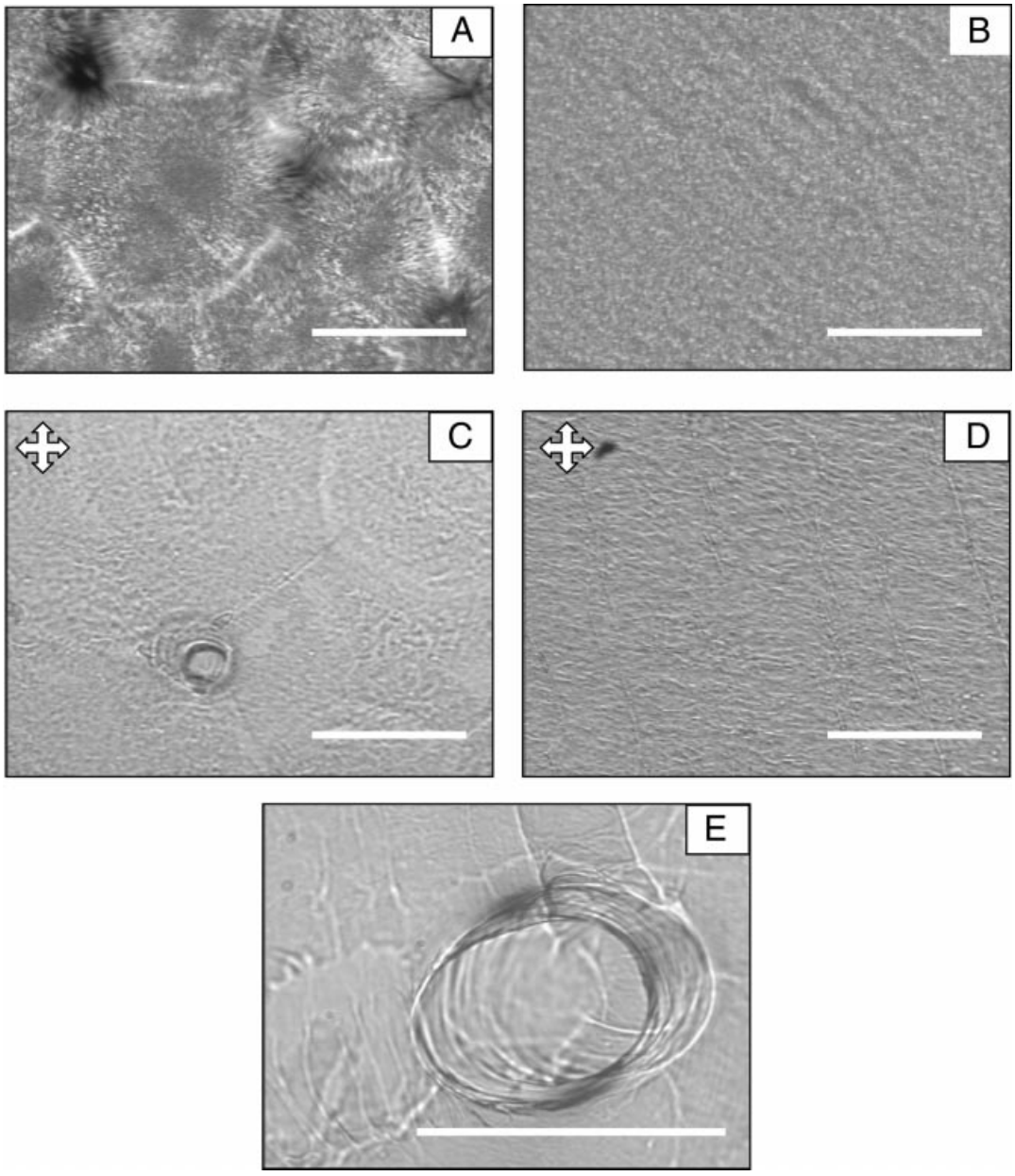


Fig. 3. Morphology from optical microscope. A: PCL-55; B: PCL-80; C: PCL-55-BXD; D: PCL-80-BXD; and E: drawing defect in PCL-55-BXD. Scale bar represents 100 μm. Biaxial drawing directions as indicated.

films at 80°C (PCL-80, Fig. 3B). The melting point of PCL polymer determined from DSC was 58°C. Hence heat pressing at 80°C effectively melts and destroys the initial spherulitic structures obtained after solution casting.

A dense fibrillar structure was observed on all samples after biaxial drawing at a draw ratio of $3 \times 3$ (Fig. 3C and D). This is expected behaviour of a semi-crystalline and rubbery material in response to tensile stresses. The fibrillar structure in PCL-80-BXD appeared to be uniformly distributed. In the PCL-55-BXD samples, the fibrils were congregated in "pockets" and bounded by what seemed remnant of the previous spherulites' boundaries. Defects-like features were also seen in the PCL-55-BXD samples. At higher magnification (Fig. 3E), these defects seemed like artefacts of non-uniform drawing, comprising of a mixture of highly drawn material and undrawn particles. These defects, however, were not found in PCL-80-BXD samples.

### *3.2. Surface morphology from atomic force microscopy*

The changes in surface morphology of PCL samples before and after biaxial drawing can be seen in Figs.4A and B, 5A and B. The surfaces appeared rather featureless after the heat pressing process.

Biaxial drawing produced fibrils in both PCL-55 and

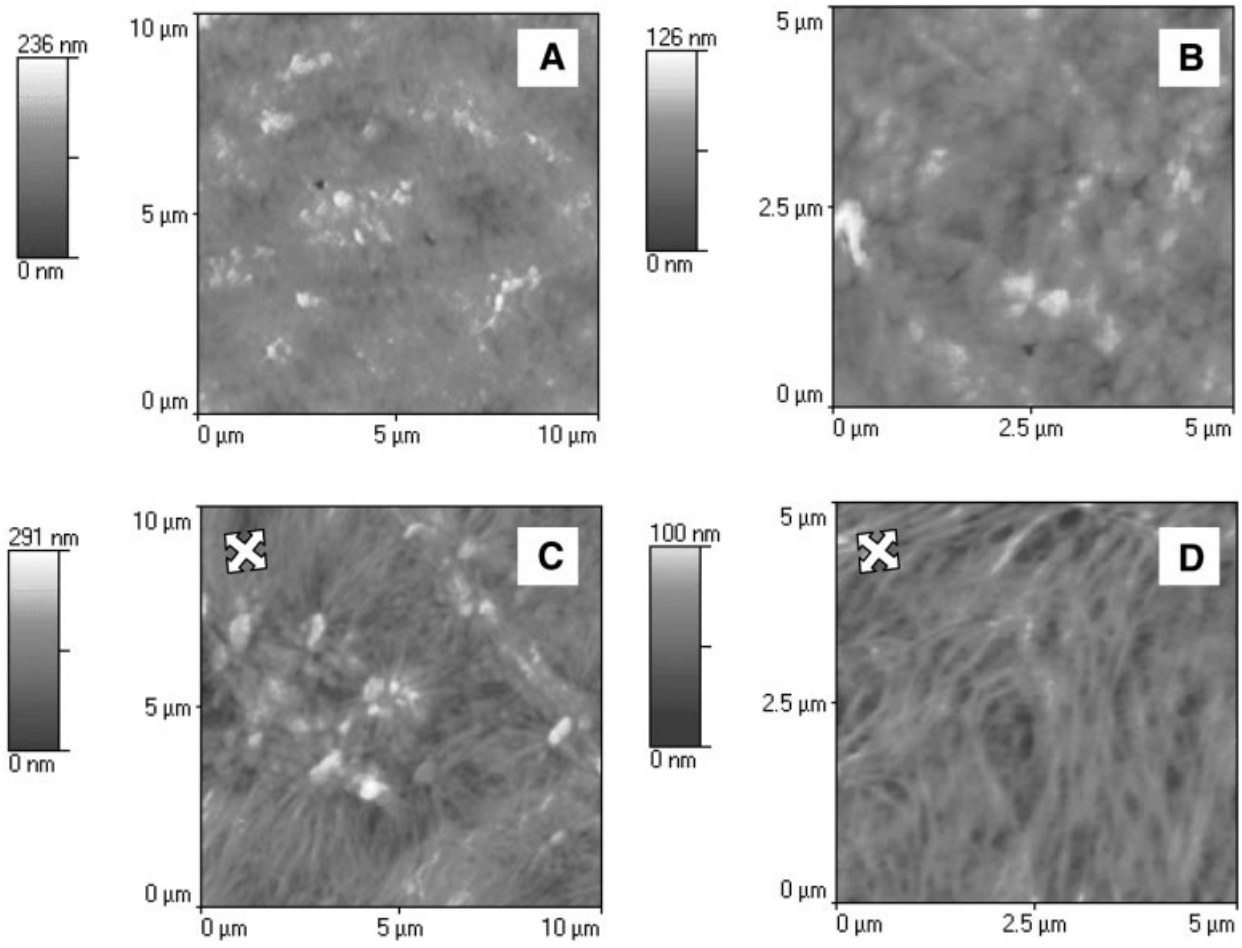


Fig. 4. AFM morphology: A and B—PCL-55; C and D—PCL-55-BXD. Biaxial drawing directions as indicated.

PCL-80 samples. However, qualitative differences between the characteristics of fibrils from the two groups could be observed. The differences are discussed in the following aspects: orientation, packing and thickness of fibrils. In the PCL-55-BXD sample, the fibrils appeared to originate from areas of undrawn material and extend outwards in all directions. This gives the appearance of a biaxial orientation (Fig. 4C). This observation is consistent with Sakai's work on biaxially drawn UHMWPE [3]. They have observed, at low draw ratios ($4 \times 4$), a mixture of fibrils and particles. In contrast, the PCL-80-BXD sample had fibrils that orient mostly in a uniaxial direction. The undrawn material looked like elongated and thick rods, rather than the spherical particles in PCL-55-BXD (Fig. 5D). It may seem that although biaxial deformation was occurring over the sample as a whole, the deformation at micro level was still uniaxial in character. This can be due to inefficient transfer of the drawing forces caused by non-uniformity, such as thickness and crystallinity variations, in the samples. In PCL-55-BXD sample, the network of fibrils appeared loose with wider gaps. In contrast, fibrils were packed closer, with fewer gaps in the PCL-80-BXD sample (Fig. 5C). The diameter of the fibrils also seemed thicker in the PCL-55-BXD sample.

### 3.3. Thermal properties from DSC

Due to the low $T_g$ of PCL, annealing of the samples, especially the PCL-80 samples, were expected during the pre-heating period before biaxial drawing. To understand the effect of the pre-heat on the crystallinity of the samples, PCL samples were annealed at 50°C for a time period ranging from 15 to 120 min. The increase in the crystallinity was followed from the change in melting enthalpy. Table 1 shows that the melting enthalpy, hence crystallinity, is stabilised after annealing for 30 min.

Fig. 6 shows the DSC trace of the PCL samples. PCL being a semi-crystalline polymer shows a very well defined melting profile. All samples melted completely at about 62°C. PCL-80 sample showed a lower melting enthalpy and peak temperature, indicating its lower crystallinity and smaller crystal lamella sizes. This was expected as the PCL specimens were melted and quenched. Crystallinity and peak temperature of PLC-80 sample increased slightly before drawing (Table 2). This was due to the annealing effect during pre-heating. Also noticed were the similar melting enthalpies of the PCL-55 and PCL-80 samples *before* drawing. Using 139.5 J/g as the melting enthalpy

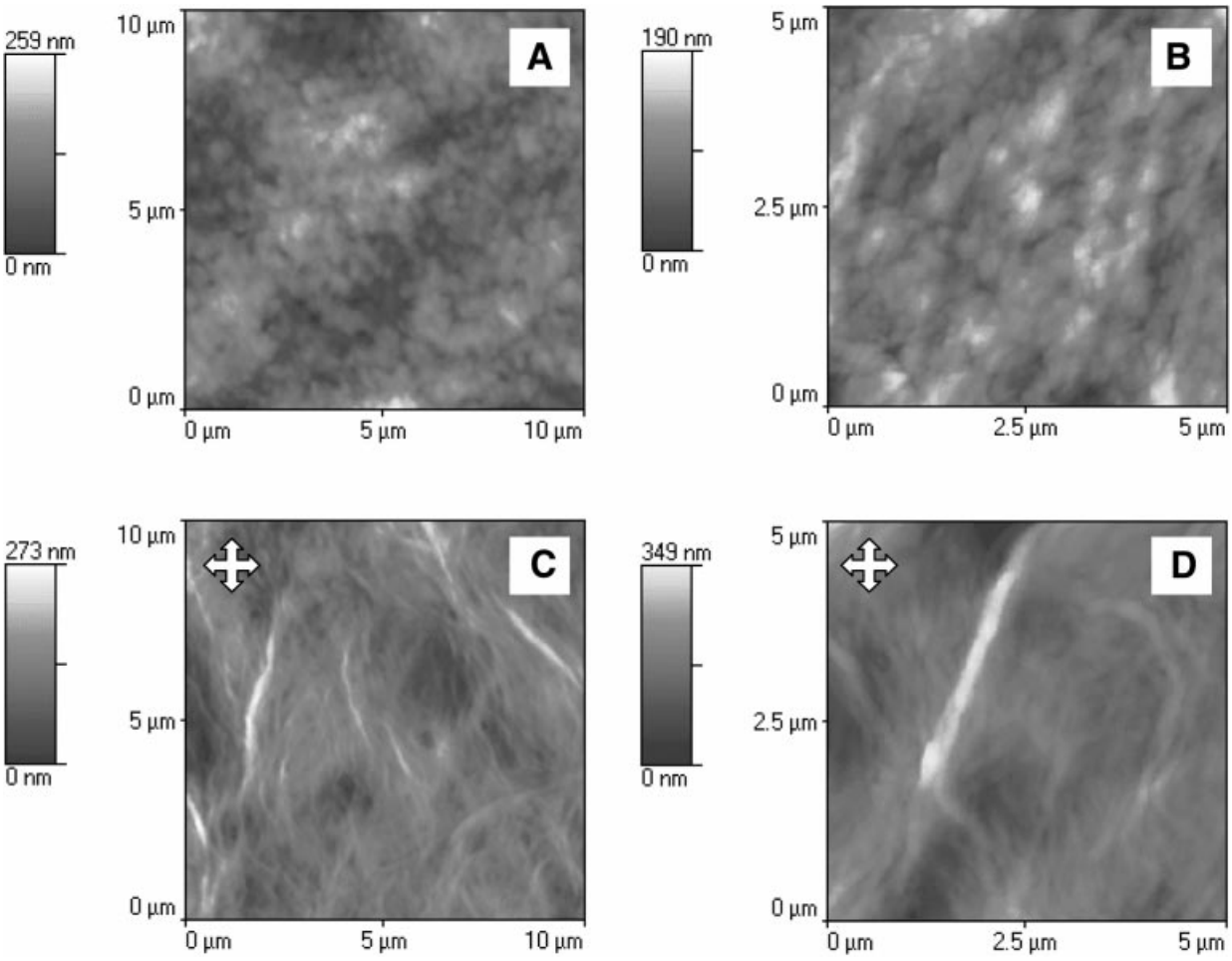


Fig. 5. AFM morphology: A and B—PCL-80; C and D—PCL-80-BXD. Biaxial drawing directions as indicated.

of 100% crystalline PCL [17], the crystallinities in both PCL samples before drawing were calculated to be about 50%.

The overall melting profiles of the biaxially drawn films became broader for both heat press temperatures. This broadening of the DSC melting peak was also observed in biaxial drawing of UHMWPE [2]. The biaxial drawing process breaks up the lamellas and widens the lamella size distribution, manifested by the broadening of the melting trace. It was also observed that a higher peak temperature of 61°C was observed for PCL-55-BXD sample. This could be due to presence of larger and/or thicker lamellas that have been formed during the drawing. Studies by Sakami et al. [2] have shown that biaxial drawing of UHMWPE produces a small amount of orthorhombic extended chain crystals having a higher melting point. PCL has a similar orthorhombic unit cell crystal structure [18] when compared with polyethylene. There are, however, no reports in relation to the drawing effects on the melting point. Crystallinity did not increase significantly after drawing as shown by the similar melting enthalpies. This was also consistent with Sakai's findings [2]. This indicates that the primary effect of biaxial drawing of PCL films at low draw ratios ($3 \times 3$) was the break up of lamellas.

Table 1
Change in melting enthalpy and peak temperature in PCL samples with annealing time. All samples annealed at 50°C

| Annealing time (min) | Melting enthalpy (J/g) | Peak temperature (°C) |
|---|---|---|
| Quenched[a] | 53 | 54 |
| 15 | 59 | 56 |
| 30 | 61 | 57 |
| 60 | 61 | 57 |
| 120 | 61 | 58 |

[a] Sample quenched in liquid nitrogen.

### 3.4. Tensile properties

The measured tensile characteristics of the PCL films are shown in Table 3. The relative Young's moduli of the films before biaxial drawing are similar. Fig. 7 displays the stress–strain plots obtained for the PCL samples. The tensile response of PCL after heat pressing is typical for a rubbery, semi-crystalline polymer. A cold-drawing stage follows after the yield point until about 400% strain. Then a strain-hardening stage comes next until film fracture.

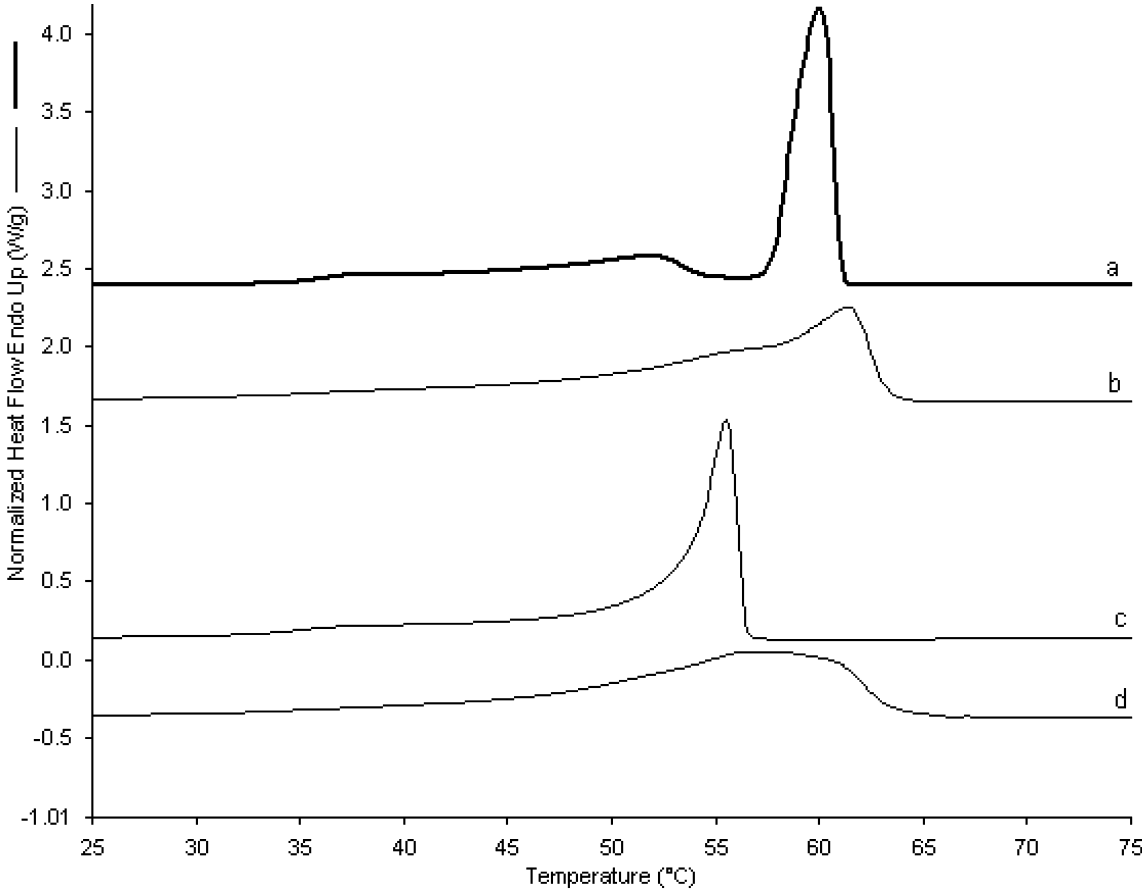


Fig. 6. DSC scans of PCL films, a—PCL-55; b—PCL-55-BXD; c—PCL-80; and d—PCL-80-BXD.

After biaxial drawing, tensile strength of the films improved for both PCL-55 and PCL-80 samples whereas elongation-at-break decreased. This improvement can be attributed to the fibrillar morphology, which is able to withstand higher mechanical loads compared to the lamellar morphology. It is also noted that PCL-55-BXD sample has a steeper strain-hardening slope than PCL-80-BXD.

On the other hand, the elongation-at-break of the PCL-55-BXD sample was lower than PCL-80-BXD. Morphology examinations have shown the presence of drawing defects in PCL-55-BXD samples. These defects are responsible for the early fracture of the PCL-55-BXD films. The high break elongations of PCL-80-BXD films shows that the draw ratio of $3 \times 3$ is rather low. As seen in AFM examinations, the drawn films still had some amount of undrawn material. This indicates the possibility of increasing the draw ratio, but alterations to the drawing instrumentation will be required to achieve this goal.

Table 2
Melting enthalpy and peak temperature of PCL films

| | Melting enthalpy (J/g) | Peak temperature (°C) |
|---|---|---|
| PCL-55 | 70 | 60 |
| PCL-55 pre-heat[a] | 71 | 60 |
| PCL-55-BXD | 71 | 61 |
| PCL-80 | 66 | 56 |
| PCL-80-pre-heat[a] | 70 | 57 |
| PCL-80-BXD | 70 | 57 |

[a] Refers to sample that was pre-heated in the chamber but not biaxially drawn yet.

### 3.5. Gas permeability

A gas may permeate through a polymer according to different mechanisms, which are determined by the polymer structure. Biaxial drawing invariably changes the polymer structure. In this study, we attempt to understand the effects of biaxial drawing on the gas permeability of PCL films.

Some of these generally known mechanisms [19] of gas transport includes Poiseuille or viscous flow, Knudsen flow and solution-diffusion process. Poiseuille flow is found in materials with defects such as pores, whose dimensions are much larger than the permeant molecules. Such materials do not show selectivity over different gases and no separation of the gases is achieved. In Knudsen flow, the gas molecules permeate through defects in the polymer whose dimensions are comparable to or larger than the mean free path of the permeant molecules, in the range of 5–1000 Å [20]. The

Table 3
Tensile properties of PCL films. Standard deviations in parentheses

| | Young's mod (MPa) | Tensile stress (MPa) | Elongation at-break (%) |
|---|---|---|---|
| PCL-55 | 276 (15) | 28 (3) | 888 (52) |
| PCL-55-BXD | 309 (13) | 42 (3) | 63 (6) |
| PCL-80 | 277 (13) | 21 (4) | 676 (57) |
| PCL-80-BXD | 273 (17) | 55 (7) | 147 (16) |

transport rate is usually determined by the molecular mass ($M_r$) of the gas molecules; it is actually related by $M_r^{-1/2}$. The solution-diffusion process is generally encountered in dense materials, where gas molecules are sorbed into the material and then diffuse through it. The rate thus depends on the solubility and diffusivity of the gas.

Table 4 shows the permeability coefficients and perm-selectivity value obtained for all PCL films tested. The PCL-55 samples have the highest gas permeabilities and $O_2/N_2$ permselectivity similar to Knudsen flow. This indicates that the gas transport in PCL-55 films is through the pores and defects in films. PCL microspheres made from solvent evaporation techniques are porous in nature. The porosity have been attributed to the presence of surface imperfections and pores due to the high crystallisation rate of PCL specimens formed by solution casting [21]. Our morphology results have shown that PCL-55 samples, although heat pressed, remained fundamentally solution-casted films. The voids from the solution casting process may have reduced in size and number due to heat pressing, but are not completely eliminated.

The permeability coefficients of PCL-80 samples were about 20 times smaller than PCL-55 samples. This is because melt pressing have reduced a large number of voids and resulted in a film denser than PCL-55. The higher-than-Knudsen permselectivity of $O_2/N_2$ indicates solution-diffusion mechanism controls the gas transport now.

The permeability of PCL films was also estimated using the Permachor approach. This method [22] uses additive molar function in estimating the permeability of polymers. The $N_2$ and $O_2$ permeability for a completely dense PCL film of 50% crystallinity was calculated and shown, together with experimental data of PCL-80, in Table 5. It is observed that the estimated values are lower than experimentally obtained ones. This suggests that the PCL-80 films may not be completely dense films; there was still presence of defects like microvoids, not eliminated during the melt pressing process. Such defects can still contribute to the gas transport via Knudsen flow mechanism, resulting in higher permeability.

### 3.6. Effect of biaxial drawing

The PCL-55-BXD samples showed a high standard deviation, indicating high variability in the permeability values. The presence of defects in the PCL-55-BXD films (Fig. 3e) were probably responsible for this variation. The lack of selectivity between $O_2$ and $N_2$ showed that gas transport was mainly viscous flow, most likely through the defects, whose dimensions were larger than 1000 Å. The measured permeability coefficients were correlated well with the defect density of the films (Table 6). Morphology examination had revealed that these defects were not pin holes but areas of non-uniformity.

PCL-80-BXD samples showed marginally higher permeabilities than PCL-80 samples. Sakai et al. [3] have reported a 1000-fold increase in $N_2$ permeability (from 1 to $10^3$ Barrer) in UHMWPE films when biaxially drawn to a draw ratio of $4 \times 4$. They attributed this increase to the formation of voids at low draw ratios.

On the other hand, Webb et al. [23] have reported, after

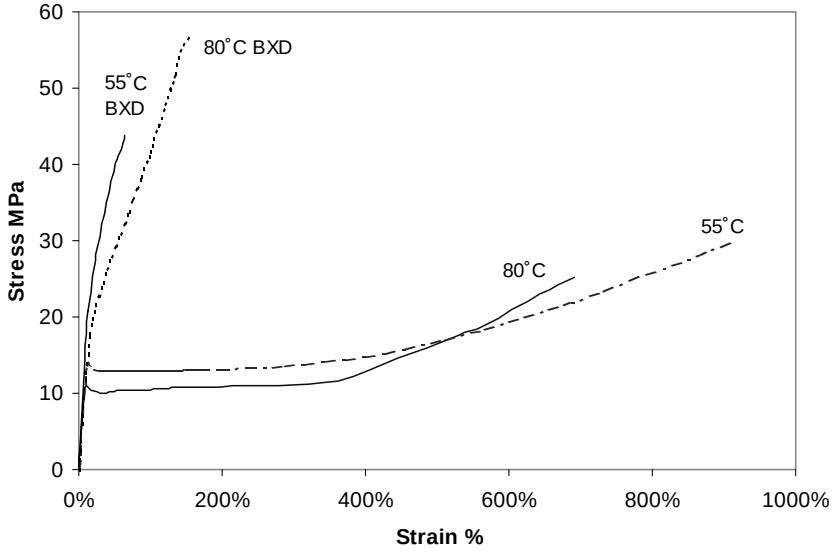


Fig. 7. Stress–strain graph of PCL films (tensile test).

Table 4
Average permeability coefficients (*P*) and permselectivities of PCL films at 25°C. Standard deviation shown in parentheses

| | *P* (Barrer)[a] | | Permselectivity |
|---|---|---|---|
| Sample | $O_2$ | $N_2$ | $O_2/N_2$ |
| | | | 0.93[b] |
| PCL-55 | 28 (4) | 30 (4) | 0.94 (0.01) |
| PCL-80 | 1.5 (0.1) | 0.52 (0.04) | 2.9 (0.1) |
| PCL-55-BXD | 21 (15) | 19 (16) | 1.1 (0.1) |
| PCL-80-BXD | 2.7 (0.6) | 0.9 (0.2) | 3.0 (0.2) |

[a] Barrer: $10^{-10}$ $cm^3$(STP)cm/$cm^2$ s cmHg.
[b] Permselectivity under pure Knudsen flow.

studying the effect of drawing on gas transport in polyethylenes, that the formation of a fibrillar structure during drawing reduces the polymer's permeability to gases. This is due to the increased tortuosity presented by the fibrillar structure.

The above two mechanisms—formation of voids and fibrillar structure—might be present in PCL-80-BXD films. At the low draw ratios used in this work, the complete fibrillar structure is not fully formed yet. Microvoids could still be present; as discussed earlier, the initial film is not completely dense. Also the breaking up of lamellaes during drawing, as shown in DSC, could create microvoids between the lamellaes and the amorphous material. It is likely that the increased permeability is due to presence of microvoids.

## 4. Conclusions

The biaxial drawing of a bioerodable polymer—PCL—has been demonstrated. Films made from solution-casting and melt pressing, were drawn to a draw ratio of $3 \times 3$. A fibrillar morphology predominated in the biaxially drawn samples although there were still presence of undrawn material. This indicates that there is a potential for a higher draw ratio that would allow the development of a complete fibrillar network. The biaxially drawn films from solution-cast samples have a looser network with thicker fibrils compared to melt-pressed films. However, in both cases, these fibrils improved the tensile strengths by 50–160%. The solution-cast films were more permeable than melt-pressed films. This was observed in both undrawn and biaxially drawn films. The gas transport mechanism in solution-cast films (undrawn and drawn) was mainly Knudsen flow, indicating diffusion through voids and drawing defects. However, melt pressing eliminated most of the voids in the PCL films and reduced the gas permeability. Oxygen was also found to permeate three times faster than nitrogen in the undrawn films. Biaxial drawing increased the gas permeability slightly but selectivity remained fairly constant. The predominant transport mechanism in melt-pressed films was solution-diffusion.

Table 5
Comparison of estimated and experimental values for permeability coefficients of PCL-80

| | *P* (Barrer) | |
|---|---|---|
| | $O_2$ | $N_2$ |
| Estimated | 0.3[a] | 0.08 |
| Experiment | 1.5 | 0.52 |

Table 6
Relation between nitrogen gas permeability (*P*) and defect density observed on PCL-55-BXD samples

| Sample no. | $P(N_2)$[a] Barrer | Defect density[b] ($mm^{-2}$) |
|---|---|---|
| 1. | 7 | 0.26 |
| 2. | 14 | 0.44 |
| 3. | 37 | 0.99 |

[a] The same trend was observed in $O_2$ permeability. Only $N_2$ data is shown here.
[b] Determined by counting the number of defects in a given area, under microscope.

## Acknowledgements

The authors appreciate the assistance from Mr Mark Chan Wai Herng for assembling the Biaxial drawing apparatus and the advice from Dr Shieh Jyh-Jeng and Ms Lin Wen Hui on the permeability data analysis. The award of a Research Scholarship by the National University of Singapore to Mr C. S. Ng is also gratefully acknowledged.

## References

[1] Hensen F. Plastics extrusion technology, New York: Hanser, 1997 chap. 8.
[2] Sakai Y, Miyasaka K. Polymer 1990;29:1608–14.
[3] Sakai Y, Miyasaka K. Polymer 1990;31:51–57.
[4] Sakai Y, Umetsu K, Miyasaka K. Polymer 1993;34:318–22.
[5] Taraiya AK, Orchard GAJ, Ward IM. Plast Rubber Composite Process Appl 1993;19:273–8.
[6] Chu F, Yamaoka T, Ide H, Kimura Y. Polymer 1994;35:3442–8.
[7] Gerrits NSJA, Lemstra PJ. Polymer 1991;32:1770–5.
[8] Zhu W, Zhang X, Zhao CT, et al. Polym Adv Technol 1996;7:743–8.
[9] Amass W, Amass A, Tighe B. Polym Int 1998;47:89–144.
[10] Sam A, Zhong PJ, Doherty SP, et al. Biomaterials 1993;14:648–56.
[11] Ory SJ, et al. Am J Obstetrics Gynecology 1983;145:600–5.
[12] Darney PD, Monroe SE, Klaisle CM, et al. Am J Obstetrics Gynecology 1989;160:1292–5.
[13] Bezwada RS, Jamiolkowski DD, Lee IY, et al. Biomaterials 1995;16:1141–8.
[14] Teoh SH, et al. J Mater Sci Mater Med 1999;10:343–52.
[15] Shieh JJ, Chung TS. J Polym Sci Part B Polym Phys 1999;37(20):2851–61.
[16] Runt J, Rim PB. Macromolecules 1982;15:1018–23.
[17] Skoglund P, Fransson A. J Appl Polym Sci 1996;61:2455–65.
[18] Hu H, Dorset DL. Macromolecules 1990;23:4604–7.
[19] Baker RW. Membrane separation systems: recent developments

and future directions, Park Ridge, NJ: USA Noyes Data Corp, 1991 chap. 3.
[20] Shilton SJ, Bell G, Ferguson J. Polymer 1996;37(3):485–92.
[21] Huatan H, Collett JH, Attwood D. J Microencapsulation 1995;12(5):557–67.
[22] Van Krevelen DW. Properties of Polymers: Their correlation with chemical structure; their numerical estimation and prediction from additive group contributions, Amsterdam: Elsevier, 1990 chap 18.
[23] Webb JA, Bower DI, Ward IM, et al. J Polym Sci Part B Polym Phys 1993;31:743–57.